CPP

WILEY-VCH

REPRINT

Analyzing Quantum Correlations Made Simple

T. Dornheim[1], **H. Thomsen**[1], **P. Ludwig**[1*], **A. Filinov**[1,2], and **M. Bonitz**[1]

[1] Institut für Theoretische Physik und Astrophysik, Christian-Albrechts-Universität zu Kiel, Leibnizstraße 15, 24098 Kiel, Germany
[2] Joint Institute for High Temperatures RAS, Izhorskaya str. 13, 125412 Moscow, Russia

The understanding of correlations in degenerate nonideal many-particle systems is complex and theoretically challenging. Using the recently proposed permutation blocking path integral Monte Carlo (PB-PIMC) scheme, which allows for an exact treatment of many-body correlations, we study the influence of quantum statistics in a confined few-particle Coulomb (quantum dot) system. As a versatile tool to gain insight into the internal structure of correlated many-body systems, the application of triple correlation functions is extended to quantum systems.

Self-organized structure formation of interacting particles is one of the most fundamental processes in nature [1]. The basic theoretical understanding and analysis of this cooperative phenomena requires (i) sophisticated simulation techniques that allow us to solve the basic equations of many-particle physics on first principles, and (ii) advanced tools for the analysis of the details of collective behaviour in these interacting systems such as structure formation, spatial correlations and melting (phase) transitions. However, even simple models used to describe interacting quantum systems in the regime where strong Coulomb correlations and quantum exchange effects are present are computationally very demanding. Therefore, trapped few-particle systems such as electrons in quantum dots [2] ("artificial atoms") serve as a suitable laboratory for the investigation of fundamental many-body interaction phenomena without requiring undesirable (uncontrollable) simplifications of the fundamental physics.

Path integral Monte Carlo (PIMC) is a finite temperature simulation technique for an ab-initio description of correlated quantum systems with arbitrarily strong Coulomb and quantum exchange (spin) effects [3, 4]. Furthermore, it provides a high flexibility with respect to trap geometry or the inclusion of defects et cetera, and quasi exact simulations with up to $N \sim 10^4$ bosons and boltzmannons are feasible [5, 6]. However, a rigorous and exact treatment of fermionic quantum exchange with standard PIMC is strongly limited by the fermion sign problem [7, 8]. For that reason, the permutation blocking path integral Monte Carlo (PB-PIMC) scheme [9, 10] has been recently introduced which allows us to significantly reduce this issue and to extend the range of application of the PIMC method towards stronger degeneracy, i.e., lower temperature and higher densities. Therefore, we are able to obtain approximation-free data for Bose, Boltzmann and Fermi statistics on the footing of first principle quantum Monte Carlo simulations.

Apart from an accurate computation, a central aspect of this contribution concerns the analysis of quantum correlations. To this end, we will extend the application of the recently derived triple-correlation functions [11–13] in order to resolve the influence of different quantum statistics on spatial correlations in degenerate 2D Coulomb (quantum dot) systems. While the (radial) pair distribution function–as a widely used tool for the structural analysis–is well suited for the investigation of the structure in homogeneous macroscopic systems with isotropic pair interaction potentials, in confined systems, where translational symmetry is lost, the distribution of pairs may depend on the position within the trap and a function that solely depends on the modulus of the pair distance does not allow for a local differentiation (e.g. between shells). For that reason, we utilize an appropriate generalized, angle resolved quantity to visualize complex spatial correlations in confined systems with an inhomogeneous density profile. The concept of such a many-body correlation function has possible applications over wide ranges:

---

* Corresponding author. E-mail: ludwig@theo-physik.uni-kiel.de

Wiley Online Library

from finite quantum systems such as electronic structures, classical systems like dusty plasma Coulomb crystals in confining potentials [11–15] or self-organized barrier discharges [16, 17], to the constellation of extragalactic objects in astrophysics [18, 19].

1   System of study

As a representative model of a strongly correlated electronic system, we consider a single quantum dot consisting of $N = 13$ charged particles in a (concentric) $2D$ harmonic confinement of frequency Ω, which is described by the dimensionless Hamiltonian

$$\hat{H} = -\frac{1}{2}\sum_{k=1}^{N}\nabla_k^2 + \frac{1}{2}\sum_{k=1}^{N}\mathbf{r}_k^2 + \sum_{k<l}^{N}\frac{\lambda}{|\mathbf{r}_k - \mathbf{r}_l|} \ . \tag{1}$$

Oscillator units (i.e., the characteristic length $l_0 = \sqrt{\hbar/m\Omega}$ and energy scale $E_0 = \hbar\Omega$) are used throughout this work. The coupling constant $\lambda = q^2/(l_0\hbar\Omega)$ (with q being the particle's charge) characterizes the strength of the Coulomb repulsion and can be controlled (experimentally) by the variation of the trap frequency. In order to analyze the characteristics of quantum exchange, we study fermions (e.g. spin-polarized electrons in a quantum dot [20–22]), bosons (e.g. indirect excitons [23, 24]), and distinguishable particles referred to as "boltzmannons", see e.g. [25]. To simulate the system at finite temperature, we are using rigorous path integral Monte Carlo methods as outlined in section 2. Here, we consider a relatively low temperature, i.e., inverse temperature $\beta = 1/k_{\mathrm{B}}T = 3$ and vary the coupling strength λ over two orders of magnitude.

2   Finite temperature quantum Monte Carlo simulations

The Path Integral Monte Carlo (PIMC) method [3] is one of the most powerful available tools for the treatment of strongly correlated and degenerate quantum systems yielding direct results for the particle density distributions that are free from any approximations or fit parameters. The only simulation input data involved are the fundamental pair (e.g. Coulomb) interaction potentials as well as the boundary (confinement) conditions allowing for a high flexibility regarding to specific setups (system's geometry, defects, external fields, etc.). PIMC is based on the Metropolis algorithm [26], which allows to generate configurations from the canonical distribution and, therefore, yields direct thermodynamic averages, i.e., finite temperature results. Despite the complexity of a physical system, the PIMC method achieves excellent performance, as long as the particles obey Boltzmann[1] or Bose statistics. In the path integral picture (i.e., the imaginary time path integral representation of the density matrix), quantum statistics requires the additional sampling of the particle permutations, which significantly increases the dimensionality of the configuration space. These permutations can be decomposed into a sequence of two-particle exchanges along the imaginary timeline. In the case of fermions, the superposition of all $N!$ permutations of N identical particles leads to the inherent[2] *fermionic sign problem*, since an alternating sign of the prefactor of the many-body density matrix causes an essential cancellation of positive and negative contributions corresponding to even and odd permutations, respectively [7]. Thus, an accurate calculation of these vanishing differences is exponentially aggravated [8] with the increase of quantum degeneracy arising at low temperatures and high densities, where all permutations appear with nearly equal probability. The recently introduced Permutation Blocking PIMC (PB-PIMC) scheme employed in this contribution allows us to overcome these severe limitations of standard PIMC and thereby to significantly extend the accessible parameter ranges of fermions towards higher degeneracy [9, 10].

---

[1] PIMC runs most efficient if quantum statistics is neglected and distinguishable spinless (Boltzmann) particles are considered [1].

[2] One has to distinguish between the cancellation of contributions inherent to the Metropolis Monte Carlo sampling scheme and the limited numerical precision due to a finite number of bits, which can be neglected here.

2.1 Standard PIMC

We consider the canonical ensemble (with fixed particle number N, trap frequency Ω and inverse temperature $\beta = 1/k_{\mathrm{B}}T$) and write the partition function for N distinguishable particles in coordinate representation as

$$Z = \int \mathrm{d}\mathbf{R} \langle \mathbf{R}| \, e^{-\beta \hat{H}} \, |\mathbf{R}\rangle \,, \tag{2}$$

with $\mathbf{R} = \{\mathbf{r}_1, \ldots, \mathbf{r}_N\}$ containing all particle coordinates. To simulate the system using the standard path integral Monte Carlo method, e.g. [3, 4], we exploit a group property of the density matrix

$$e^{-\beta \hat{H}} = \left(e^{-\epsilon \hat{H}} \right)^P \,, \tag{3}$$

with $\epsilon = \beta/P$, and insert $P - 1$ unities of the form $\hat{1} = \int \mathrm{d}\mathbf{R}_\alpha \, |\mathbf{R}\rangle_\alpha \langle \mathbf{R}|_\alpha$ to transform Eq. (2) to

$$Z = \int \mathrm{d}\mathbf{X} \, \langle \mathbf{R}_0| \, e^{-\epsilon \hat{H}} \, |\mathbf{R}_1\rangle\langle \mathbf{R}_1| \, \cdots \, |\mathbf{R}_{P-1}\rangle\langle \mathbf{R}_{P-1}| \, e^{-\epsilon \hat{H}} \, |\mathbf{R}_0\rangle \,, \tag{4}$$

with the integration being carried out over P sets of coordinates, $\mathrm{d}\mathbf{X} = \mathrm{d}\mathbf{R}_0 \ldots \mathrm{d}\mathbf{R}_{P-1}$. Eq. (4) is exact and constitutes an integral over P density matrices at P times the temperature. This allows one to use the *primitive approximation* $e^{-\epsilon \hat{H}} \approx e^{-\epsilon \hat{K}} e^{-\epsilon \hat{V}}$, with $\hat{K}$ and $\hat{V}$ being the kinetic and potential contribution to the Hamiltonian, respectively, which yields exact results for $P \to \infty$. The separate matrix elements of $e^{-\epsilon \hat{V}}$ and $e^{-\epsilon \hat{K}}$ are known, and the resulting high-dimensional integral can be evaluated using the Metropolis algorithm [26]. To simulate bosons or fermions, one has to extend the partition function by the sum over all permutations

$$Z = \frac{1}{N!} \sum_{\sigma \in S_N} \mathrm{sgn}(\sigma) \int \mathrm{d}\mathbf{R} \, \langle \mathbf{R}| \, e^{-\beta \hat{H}} \, |\hat{\pi}_\sigma \mathbf{R}\rangle \,, \tag{5}$$

with $\hat{\pi}_\sigma$ being the exchange operator which corresponds to a particular element σ from the permutation group S_N. Hence, Eq. (5) requires the employed PIMC approach to generate exchange cycles, which can be very efficiently accomplished using the worm algorithm [5, 6]. For bosons and boltzmannons, all terms are strictly positive. However, the sign of fermionic contributions depends on the parity of the particular permutation. With increasing exchange effects, towards high density and low temperature, permutation cycles with positive and negative signs appear with nearly equal probability and, therefore, the statistical error increases exponentially. This numerical issue is known as the *fermion sign problem* [7] and limits standard PIMC to weak degeneracy, i.e., strong coupling and/or high temperature, where exchange effects play only a minor role.

2.2 Permutation Blocking PIMC

PB-PIMC is basically a combination of (i) antisymmetric imaginary time propagators, i.e., determinants [27–29], which allow for an analytic cancellation of positive and negative permutations within a single configuration weight (permutation blocking), (ii) a higher-order factorization of the density matrix [30–32], and (iii) a highly efficient Monte Carlo sampling scheme based on artificial trajectories [9]. While the blocking of permutations can lead to a significant reduction of the fermion sign problem, with an increasing number of propagators P this advantage quickly vanishes. Therefore, instead of the *primitive approximation*, the PB-PIMC implementation utilizes the *fourth order factorization* [31, 32]

$$e^{-\epsilon \hat{H}} \approx e^{-v_1 \epsilon \hat{W}_{a_1}} e^{-t_1 \epsilon \hat{K}} e^{-v_2 \epsilon \hat{W}_{1-2a_1}} e^{-t_1 \epsilon \hat{K}} e^{-v_1 \epsilon \hat{W}_{a_1}} e^{-2t_0 \epsilon \hat{K}} \quad , \tag{6}$$

of the density matrix, which allows for sufficient accuracy with only a few high temperature factors. The $\hat{W}$ operators in Eq. (6) denote a modified potential, which combines $\hat{V}$ with double commutator terms of the form [32]

$$[[\hat{V}, \hat{K}], \hat{V}] = \frac{\hbar^2}{m} \sum_{i=1}^{N} |\mathbf{F}_i|^2 \,. \tag{7}$$

Therefore, PB-PIMC requires the evaluation of the force acting on each particle $\mathbf{F}_i = -\nabla_i V(\mathbf{R})$. The final result for the partition function is given by

$$Z = \frac{1}{(N!)^{3P}} \int \mathrm{d}\mathbf{X} \prod_{\alpha=0}^{P-1} e^{-\epsilon \tilde{V}_\alpha} e^{-\epsilon^3 u_0 \frac{\hbar^2}{m} \tilde{F}_\alpha} \det(\rho_\alpha) \det(\rho_{\alpha A}) \det(\rho_{\alpha B}) \,, \tag{8}$$

with $\tilde{V}_\alpha$ and $\tilde{F}_\alpha$ containing the contributions of the potential and the forces, respectively, and the diffusion matrix

$$\rho_\alpha(i,j) = \lambda_{t_1\epsilon}^{-D} \exp\left(-\frac{\pi}{\lambda_{t_1\epsilon}^2} (\mathbf{r}_{\alpha,j} - \mathbf{r}_{\alpha A,i})^2 \right) \,, \tag{9}$$

with $\lambda_{t_1\epsilon} = \sqrt{2\pi\epsilon t_1 \hbar^2/m}$ being the thermal wavelength of a single time slice. Instead of explicitly sampling each permutation cycle as in standard PIMC, we combine configuration weights of both positive and negative sign in the determinants, which leads to a cancellation of terms and, therefore, a highly effective blocking of permutations. When the wavelength $\lambda_{t_1\epsilon}$ is comparable to the mean inter-particle distance, the blocking is most effective and the average sign in the Monte Carlo simulations is significantly increased. However, with an increasing P, $\lambda_{t_1\epsilon}$ decreases and, eventually, the average sign converges towards the sign from standard PIMC. Hence, it is crucial to employ the fourth order factorization from Eq. (6), which allows for sufficient accuracy with as few as two or three propagators. To ensure an ergodic and highly efficient sampling procedure for this modified configuration space, we have combined the worm algorithm idea [6] with the temporary construction of artificial trajectories where blocking happens automatically as a by-product. For a detailed description of PB-PIMC, we refer to [9].

For the sake of completeness, we mention that the recently introduced Configuration PIMC (CPIMC) approach [33–35] exhibits a complementary range of applicability ($\lambda \lesssim 1$). CPIMC can be interpreted as a Monte Carlo simulation on an expansion around the ideal system and, therefore, excels at weak coupling and strong degeneracy. Unfortunately, the physically most interesting transition region remains out of reach. A popular extension of standard PIMC towards higher degeneracy is Restricted PIMC (RPIMC), often denoted as fixed node approximation [36]. However, this approach requires explicit knowledge of the nodal structure of the density matrix, which is a priori unknown. Therefore, one has to rely on approximations which introduce an uncontrolled systematic error [37, 38]. To circumvent these issues, here we pursue the above introduced permutation blocking idea which allows us to simulate the system over the entire coupling range.

3 Particle distribution functions

Microscopic phase-space information, and in particular the distribution of particles and particle pairs are central quantities in statistical physics. While the radial pair distribution function $g(r) = g(|\mathbf{r}_2 - \mathbf{r}_1|)$ is well suited for the analysis of the structure in homogeneous isotropic systems, see e.g. [39], an advanced quantity is required for confined systems. In the homogeneous system, the two-particle distribution $\rho_2(\mathbf{r}_1, \mathbf{r}_2)$ must not depend on the position of the particle pair or on its orientation due to the symmetry. Hence, the pair correlations can be described solely as a function of the absolute pair distance r.

3.1 Two-particle density

For a harmonically trapped system, ρ_2 is not invariant under translation, but under rotation with respect to the trap center. Consequently, an appropriate pair correlation function requires three coordinates: r_I and r_II as the radial position of the first and the second particle of the pair, respectively, and the enclosed angle ϑ with respect to the trap center, cf. Fig. 1. The two-particle density in generalized coordinates $\rho_2(r_\mathrm{I}, r_\mathrm{II}, \vartheta)$ is sampled as a three-dimensional histogram in the PIMC simulation. This quantity is referred to as *center-two-particle* (c2p) density and can be interpreted as the probability of measuring a pair of particles of which the first (second) has a distance r_I (r_II) from the trap center and where both particles enclose an angle ϑ with the trap center, cf. Fig. 1.
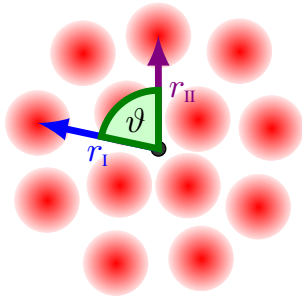
Fig. 1 Generalized coordinates of the center-two-particle correlation function $\rho_2(r_{\mathrm{I}}, r_{\mathrm{II}}, \vartheta)$ for a harmonically confined 2D Coulomb cluster. All possible positions of two particles are sampled and compiled with respect to three parameters: distance r_{I} of the first particle from the trap center, distance r_{II} of the second particle from the trap center, and their connecting angle ϑ. In the *center-two-particle* distribution function, the trap center serves as a third reference point. The classical particle positions serve as an example, where the $N = 13$ particles arrange themselves on two concentric shells.

3.2 Two-particle correlations

In order to emphasize angular correlations, it has proven reasonable to define the *center-two-particle* (c2p) correlation function

$$g_{\mathrm{c2p}}(r_{\mathrm{I}}, r_{\mathrm{II}}, \vartheta) = \frac{\rho_2(r_{\mathrm{I}}, r_{\mathrm{II}}, \vartheta)}{\rho_2^{\mathrm{id}}(r_{\mathrm{I}}, r_{\mathrm{II}}, \vartheta)}, \tag{10}$$

which is normalized by the *ideal two-particle density* ρ_2^{id} of a corresponding system with the same radial density profile but without any angular modulations. This allows one to compensate for the non-correlation related effects that are solely caused by the inhomogeneous density profile. For 2D systems, this density is given by[3] $\rho_2^{\mathrm{id}} = \frac{N-1}{N} 4\pi r_{\mathrm{I}} r_{\mathrm{II}} n(r_{\mathrm{I}}) n(r_{\mathrm{II}})$ as the product of the radial density $n(r)$ at both particle radii [11–13].

While $g_{\mathrm{c2p}}(r_{\mathrm{I}}, r_{\mathrm{II}}, \vartheta)$ is a function of three coordinates, a two-dimensional distribution function $g_{\mathrm{c2p}}^{\mathrm{int}}(r_{\mathrm{II}}, \vartheta)$ is extracted by the integration over a particular r_{I} range. Here, we have integrated over an r_{I} range that corresponds to the outer (inner) shell or region when the shell structure has vanished. For classical or localized quantum particles, this can be interpreted as choosing one reference particle from the outer (inner) shell.

Being derived from the concept of a many-particle correlation function, the c2p function takes explicitly into account the concentric symmetry of the harmonically confined system. It provides local insight into the structure and allows one to resolve the radial and relative angular distribution of two particles with respect to the trap center. In particular, it is sensitive to the mutual orientation of particle pairs, but not affected by a rotation of the particle cluster as a whole (e.g. during the simulation run). The c2p function is well defined and robust yielding reliable information also in the case of partially incomplete data sets, e.g. from experiments. As this quantity relies only on the statistical distribution of particle positions, it does neither require explicitly labeled particles nor dynamical information such as particle trajectories, which makes the c2p function well suited for equilibrium Monte Carlo simulations.

4 Analysis of spatial quantum correlations

Considering Bose, Boltzmann and Fermi statistics for a system of $N = 13$ particles, we investigate the influence of quantum statistics on the spatial correlations over a wide range of the coupling parameter λ covering two orders of magnitude.

Figure 2 shows the integrated c2p-density where we have carried out the r_{I}-integration over the outer region of the system (shaded area in the inset density profile). The first column shows a strongly coupled system ($\lambda = 10$). Due to the strong Coulomb repulsion, the particles are quasi localized and the quantum statistics has only a small influence on the structure because of the negligible overlap of the wave function. The radial density (top panel and black line in the insets) is virtually the same for all three particle types and exhibits two distinct shells. In parts (a), (d) and (g) of Fig. 2, the c2p correlation function reveals no significant differences between the three systems as well. The most prominent feature is the correlation hole at a radial coordinate $r_{\mathrm{II}} \approx 4$ and small angular pair distances $\vartheta \lesssim 30°$.

---

[3] The factor $(N-1)/N$ is conventional and ensures that the normalization of both ρ_2 and ρ_2^{id} is the number of particle pairs. The factor has only minor influence on the result especially for large particle numbers. It has no qualitative impact on the structures which are found in the plots. For small particle numbers, one finds that with the factor included, g_{c2p} approaches a value slightly above unity for large distances and weak correlations, cf. bottom row of Fig. 2. This can be understood since the correlation hole at small distances has to be compensated.
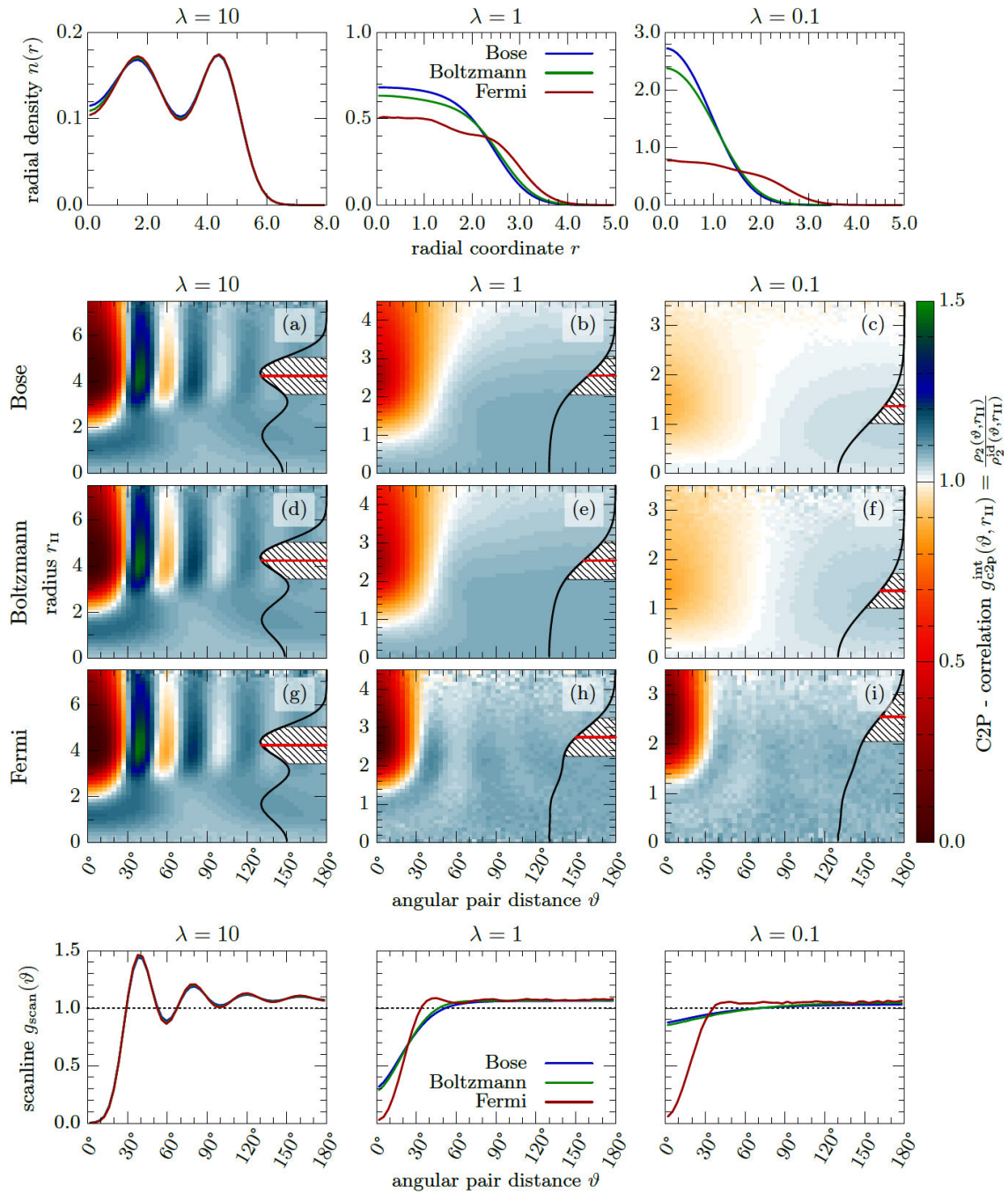
Fig. 2 Effect of quantum statistics in the outer shell: <u>Center panel</u>: center-two-particle correlation function for a system of $N = 13$ bosons, boltzmannons, and fermions at strong ($\lambda = 10$), moderate ($\lambda = 1$) and weak ($\lambda = 0.1$) coupling strength. The radial density is shown as an inset where the shaded area indicates the r_{I} integration range. The red line indicates the angular density cut (scanline) through the outer shell which is shown in the lower panel. <u>Top panel</u>: comparison of the radial density profiles for the three different statistics. <u>Bottom panel</u>: scanlines through the r_{II}-ϑ plane as indicated by the red line in (a-i) at constant r_{II}.

This hole is followed by a sequence of maxima and minima in ϑ direction which correspond to angular pair correlations within the outer shell. These correlations are found even for distant particles with $\vartheta \approx 180°$, i.e.,

the particles are located at opposite sides of the trap. Since it is difficult to meter the absolute height in color maps, we show a scanline at the middle of the outer shell in the bottom panel. This scanline $g_{\text{scan}}(\vartheta)$ confirms that virtually the same intra-shell angular correlations are found for bosons, boltzmannons and fermions at strong coupling. As a further interesting feature in panels (a), (d) and (g), we find angular correlations with the particles on the inner shell, which appear as–less pronounced–maxima and minima at a radius $r_{\text{II}} \approx 1.5$ that corresponds to the inner shell. This means that orientations of inner and outer shell are not independent.
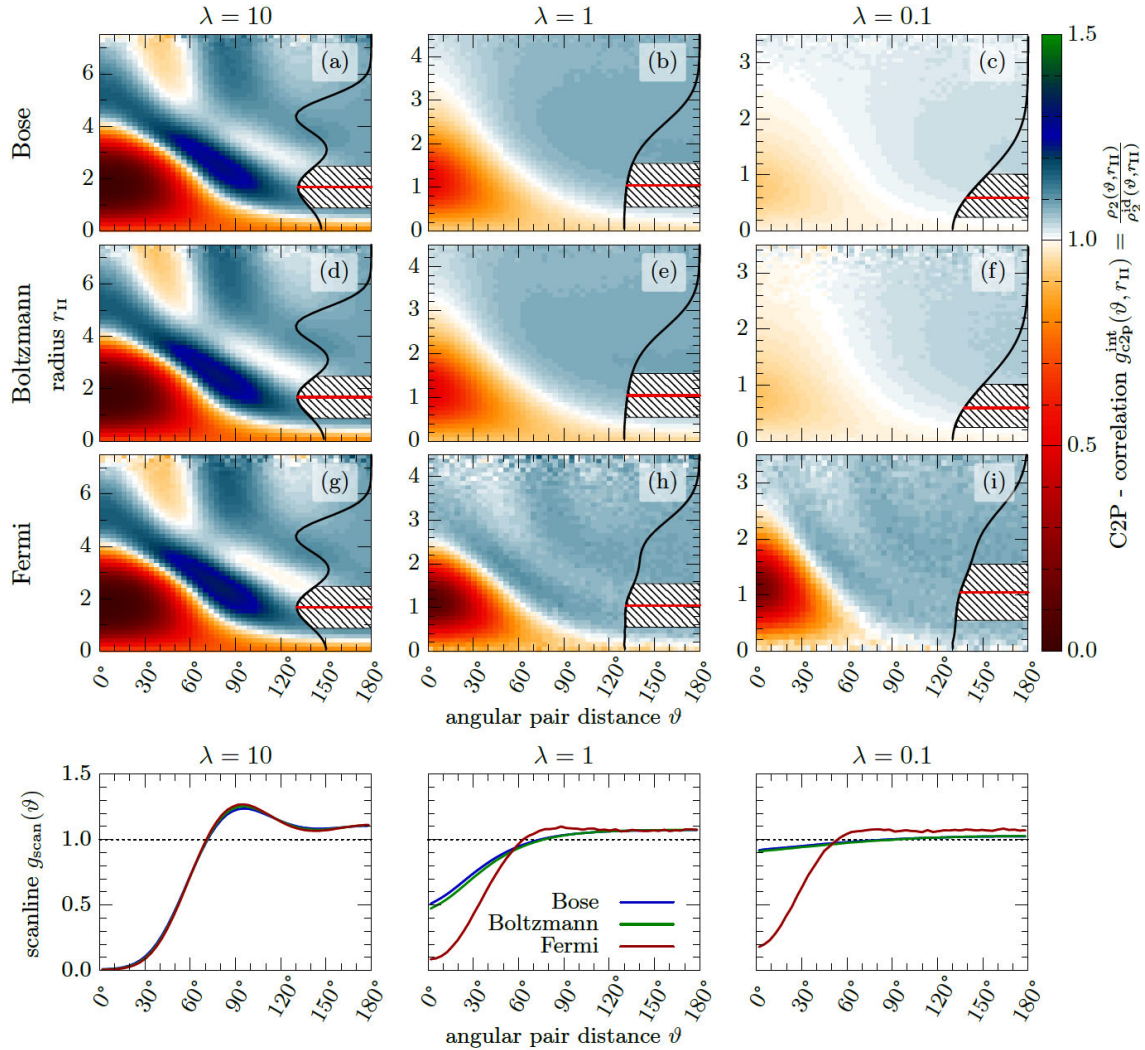
Fig. 3 Effect of quantum statistics in the inner shell: Center-two-particle correlation function (top panel) as in Fig. 2 but with r_{I} being integrated over the inner region (shaded area in the inset). The scanlines (bottom panel) at the r_{II} value which is marked by the red line show the intra-shell angular correlations within the inner shell.

At a ten times lower coupling parameter ($\lambda = 1$) shown in the central column of Fig. 2, the quantum statistics has a noticeable impact on the spatial structure of the systems. In the radial density shown at the top panel, we find that the cluster of fermions is enlarged compared to bosons and boltzmannons because of the degeneration pressure. In parts (b), (e) and (h), the c2p correlation function again shows the correlation hole[4] around $r_{\text{II}} = 3$ and small angular pair distances ϑ for all three quantum statistics. As a unique feature, the fermionic system exhibits angular correlations also at larger distances. These appear as a sequence of dark and bright areas along

---

[4] For fermions, the correlation hole is caused by both quantum exchange effects and the Coulomb repulsion. In this case, one might refer to this as an exchange correlation hole.

the direction of ϑ. In the scanline (bottom panel), the angular correlations beyond the correlation hole at $\vartheta = 0°$ are reflected as a maximum around $\vartheta = 40°$ followed by a minimum around $\vartheta = 60°$[5]. This feature is a manifestation of the Pauli blocking which leads to an effective 'hard-core' repulsion. The 'hard-core' interaction separates the fermions in addition to the Coulomb repulsion that is present for all three types of particles.

The right column of Fig 2 shows the three systems at weak coupling ($\lambda = 0.1$). Here, the radial density (top panel) shows that both bosons and boltzmannons concentrate at the trap center while the radial profile of the fermionic system does not change significantly compared with $\lambda = 1.0$. For bosons and boltzmannons, hardly any angular correlations are visible at weak coupling. Solely the correlation hole at small pair angles remains as a shallow minimum in parts (c) and (f) of Fig. 2. The scanline (bottom panel) reveals that the total variation of the pair density is below 20 %. In contrast, the fermionic system in part (i) of the figure exhibits clear angular correlations although these are weaker than in part (h) at moderate coupling. The scanline clearly indicates the difference between fermions on the one hand and bosons and boltzmannons on the other hand. Only the fermionic system has a pronounced (exchange) correlation hole where the correlation function drops almost down to zero which is due to the governing effect of Fermi repulsion[6].

Figure 3 displays, as a supplement for Fig. 2, the analogous function with an r_{I} integration that corresponds to the radial range of the inner instead of the outer shell. In that case, the angular correlations within the inner shell are visible as pronounced peaks around $r_{\mathrm{II}} \approx 1.5$ while very weak inter-shell angular correlations are found as weaker peaks around $r_{\mathrm{II}} \approx 5$. The inner shell is populated by $N_1 = 4$ particles on average which explains why the peak for nearest on-shell neighbors appears at $\vartheta = 90°$. For classical particles at zero temperature with such a configuration, one would expect another maximum around $r_{\mathrm{II}} \approx 1.5$ and $\vartheta = 180°$ caused by the opposite particle within the inner shell, cf. Fig. 1. Both to the quantum mechanical delocalization and the finite temperature cause the maximum to be smeared out. For this reason, the minimum at $\vartheta = 135°$ in the scanline (bottom panel) as well as the maximum at $180°$ are both very weak. Overall, we again find a crossover from a nearly classical system at strong coupling ($\lambda = 10$) towards a degenerate quantum system, where for fermions the Pauli blocking dominates. This leads to a significantly different behaviour in comparison to bosons and boltzmannons.

5 Conclusion

As a main goal, in this contribution we have investigated the influence of quantum statistics on spatial correlations in a degenerate 2D quantum dot system. Using state of the art quantum Monte Carlo techniques to simulate bosons, boltzmannons and fermions from first principles, we have studied the crossover from a nearly classical system with governing repulsive Coulomb interaction towards a density (coupling) regime that is dominated by quantum exchange effects. To resolve this effect in great detail, we have used the recently introduced center two-particle correlation function [13] which allows to study spatial many-body correlations on a level widely beyond the standard radial pair distribution function $g(r)$. A future application of this quantity may include the investigation of the spatial distribution of superfluidity in finite systems [40–42]. Furthermore, we note that a reduced entropy can be directly computed from the proposed correlation function, which is well suited to determine various kinds of phase boundaries (such as multistage intra-shell, inter-shell, and radial melting transitions) in both finite and macroscopic systems [12, 13]. In contrast to the Lindemann parameter, it is a thermodynamic quantity and therefore directly accessible to equilibrium Monte Carlo simulations as it does not require any dynamical information [1, 43].

---

[5] Two further maxima around $\vartheta = 80°$ and $\vartheta = 120°$ as well as a minimum around $\vartheta = 105°$ are clearly visible only in Fig. 2 (h). The reason for this is that the color map offers a wider overview which is missing in the scanline that includes only one bin in r_{II} direction.

[6] The reason why $g_{\mathrm{scan}}(\vartheta)$ is not exactly zero at small ϑ is the finite integration range for r_{I}. Therefore, two particles can be aligned in radial direction, i.e. $\vartheta = 0°$ and still have finite distance.

References

[1] P. Ludwig, Structure Formation in Strongly Correlated Few-Particle Systems in Traps, PhD Thesis, Universität Rostock (2008).

[2] S. Reimann, and M. Manninen, Rev. Mod. Phys. **74**, 1283 (2002).

[3] D.M. Ceperley, Rev. Mod. Phys. **67**, 279 (1995).

[4] A.V. Filinov, J. Böning and M. Bonitz, Path integral Monte Carlo simulation of charged particles in traps, in "Computational Many-Particle Physics", H. Fehske, R. Schneider and A. Weiße (Eds.), Lecture Notes in Physics **739**, Springer Heidelberg (2007).

[5] M. Boninsegni, N. Prokof'ev and B. Svistunov, Phys. Rev. Lett. **96**, 070601 (2006).

[6] M. Boninsegni, N.V. Prokov'ev and B.V. Svistunov, Phys. Rev. E **74**, 036701 (2006).

[7] E.Y. Loh, J.E. Gubernatis, R.T. Scalettar, S.R. White, D.J. Scalapino, and R.L. Sugar, Phys. Rev. B **41**, 9301 (1990).

[8] M. Troyer and U.J. Wiese, Phys. Rev. Lett. **94**, 170201 (2005).

[9] T. Dornheim, S. Groth, A. Filinov and M. Bonitz, New J. Phys. **17**, 073017 (2015).

[10] T. Dornheim, T. Schoof, S. Groth, A. Filinov, and M. Bonitz, J. Chem. Phys. **143**, 204101 (2015).

[11] H. Thomsen, J. Schablinski, and M. Bonitz, Phase Transitions in Dusty Plasmas, in "Complex Plasmas", M. Bonitz, J. Lopez, K. Becker and H. Thomsen (Eds.), Springer Series on Atomic; Optical and Plasma Physics **82**, 3 (2014).

[12] H. Thomsen and M. Bonitz, Phys. Rev. E **91**, 043104 (2015).

[13] H. Thomsen, Melting Processes and Laser Manipulation of Strongly Coupled Yukawa Systems, PhD Thesis, Christian-Albrechts-Universität zu Kiel (2015).

[14] P. Ludwig, H. Thomsen, K. Balzer, A. Filinov, and M. Bonitz, New J. Phys. **52**, 124013 (2010).

[15] A. Schella, , T. Miksch, A. Melzer, J. Schablinski, D. Block, A. Piel, H. Thomsen, P. Ludwig, and M. Bonitz, Phys. Rev. E **84**, 056402 (2011).

[16] R. Wild and L. Stollenwerk, EPJ D **66**, 214 (2012).

[17] M. Bogaczyk, S. Nemschokmichal, R. Wild, L. Stollenwerk, R. Brandenburg, J. Meichsner, and H.-E. Wagner, Contrib. Plas. Phys. **52**, 847 (2012).

[18] Edward J. Groth, and P.J. E. Peebles, ApJ **217**, 385 (1977).

[19] J.N. Fry and P.J.E. Peebles, ApJ **221**, 19 (1978).

[20] R. Egger, W. Häusler, C.H. Mak, and H. Grabert, Phys. Rev. Lett. **82**, 3320 (1999).

[21] A.V. Filinov, M. Bonitz, and Y.E. Lozovik, Phys. Rev. Lett. **86**, 3851 (2001).

[22] A. Ghosal, A.D. Güclü, C.J. Umrigar, D. Ullmo, and H.U. Baranger, Phys. Rev. B **76**, 085341 (2007).

[23] J. Böning, A. Filinov, and M. Bonitz, Phys. Rev. B **84**, 075130 (2011).

[24] K. Sperlich, P. Ludwig, A. Filinov, M. Bonitz, H. Stolz, D. Hommel, and A. Gust, phys. stat. sol. (c) **6**, 551 (2009).

[25] B.K. Clark, M. Casula, and D.M. Ceperley, Phys. Rev. Lett. **103**, 055701 (2009).

[26] N. Metropolis, A.W. Rosenbluth, M.N. Rosenbluth, A.H. Teller, and E. Teller, J. Chem. Phys. **21**, 1087 (1953).

[27] M. Takahashi and M. Imada, J. Phys. Soc. Jpn. **53**, 963 (1984).

[28] V.S. Filinov, M. Bonitz, V.E. Fortov, W. Ebeling, P. Levashov, and M. Schlanges, Contrib. Plasma Phys. **44**, 388 (2004).

[29] A.P. Lyubartsev, J. Phys. A: Math. Gen. **38**, 6659 (2005).

[30] S.A. Chin, Phys. Rev. E **91**, 031301(R) (2015).

[31] S.A. Chin and C.R. Chen, J. Chem. Phys. **117**, 1409 (2002).

[32] K. Sakkos, J. Casulleras, and J. Boronat, J. Chem. Phys. **130**, 204109 (2009).

[33] T. Schoof, M. Bonitz, A.V. Filinov, D. Hochstuhl, and J.W. Dufty, Contrib. Plasma Phys. **51**, 687 (2011).

[34] T. Schoof, S. Groth, and M. Bonitz, Optical and Plasma Physics **82**, 153 (2014).

[35] T. Schoof, S. Groth, J. Vorberger, and M. Bonitz, Phys. Rev. Lett. **115**, 130402 (2015).

[36] D.M. Ceperley, J. Stat. Phys. **63**, 1237 (1991).

[37] V.S. Filinov, J. Phys. A: Math. Gen. **34**, 1665 (2001).

[38] V.S. Filinov, High Temp. **52**, 615 (2014).

[39] P. Gori-Giorgi, F. Sacchetti, and G.B. Bachelet, Phys. Rev. B **61**, 7353 (2000).

[40] Y. Kwon, F. Paesani, and K. Whaley, Phys. Rev. B **74**, 174522 (2006).

[41] A. Filinov, J. Böning, M. Bonitz, and Yu. Lozovik, Phys. Rev. B **77**, 214527 (2008).

[42] T. Dornheim, A. Filinov, and M. Bonitz, Phys. Rev. B **91**, 054503 (2015).

[43] J. Böning, A. Filinov, P. Ludwig, H. Baumgartner, M. Bonitz, and Yu.E. Lozovik, Phys. Rev. Lett. **100**, 113401 (2008).